Determination of the Neutron Skin of ^{208}Pb from Ultrarelativistic Nuclear Collisions

Giuliano Giacalone,[1] Govert Nijs,[2] and Wilke van der Schee[3,4]
[1]Institut für Theoretische Physik, Universität Heidelberg, Philosophenweg 16, 69120 Heidelberg, Germany
[2]Center for Theoretical Physics, Massachusetts Institute of Technology, Cambridge, Massachusetts 02139, USA
[3]Theoretical Physics Department, CERN, CH-1211 Genève 23, Switzerland
[4]Institute for Theoretical Physics, Utrecht University, 3584 CC Utrecht, The Netherlands

(Received 15 June 2023; accepted 29 September 2023; published 15 November 2023)

Emergent bulk properties of matter governed by the strong nuclear force give rise to physical phenomena across vastly different scales, ranging from the shape of atomic nuclei to the masses and radii of neutron stars. They can be accessed on Earth by measuring the spatial extent of the outer skin made of neutrons that characterizes the surface of heavy nuclei. The isotope ^{208}Pb, owing to its simple structure and neutron excess, has been in this context the target of many dedicated efforts. Here, we determine the neutron skin from measurements of particle distributions and their collective flow in ^{208}Pb + ^{208}Pb collisions at ultrarelativistic energy performed at the Large Hadron Collider, which are mediated by interactions of gluons and thus sensitive to the overall size of the colliding ^{208}Pb ions. By means of state-of-the-art global analysis tools within the hydrodynamic model of heavy-ion collisions, we infer a neutron skin $\Delta r_{np} = 0.217 \pm 0.058$ fm, consistent with nuclear theory predictions, and competitive in accuracy with a recent determination from parity-violating asymmetries in polarized electron scattering. We establish thus a new experimental method to systematically measure neutron distributions in the ground state of atomic nuclei.

DOI: 10.1103/PhysRevLett.131.202302

Understanding the distribution of neutrons within heavy atomic nuclei has profound implications for our knowledge of the neutron-rich matter that shapes exotic astrophysical objects such as neutron stars. The neutron skin that forms on the surface of heavy nuclei, whereby neutrons are located more diffusely and more on the outside [1,2], represents in particular a sensitive probe of the equation of state (EOS) of neutron matter, whose pressure determines the spatial extent of the neutron distributions. Indeed, nuclear models predict a strong correlation between the neutron skins of heavy nuclei and the masses and radii of neutron stars [3,4].

While proton distributions in nuclei can be determined in a model-independent way from electron scattering experiments [5], accessing neutron distributions poses a far greater challenge. As a consequence, we have only limited experimental constraints on the neutron skin of nuclei, Δr_{np}, defined as the difference in root mean square (rms) radii between protons and neutrons. The doubly magic nucleus ^{208}Pb ($Z = 82$, $N = 126$) has both protons and neutrons filling up their respective shells and represents an optimal study subject in this context. A recent, precise deduction of the neutron skin of ^{208}Pb has been achieved by the PREX Collaboration [6] from the measurement of parity-violating asymmetries in polarized electron scattering. On the side of theory, the first calculation of ^{208}Pb and its neutron skin in the context of *ab initio* nuclear theory was also recently performed [7]. These results, along with information coming from pulsar and gravitational wave observations, portray a picture of nuclear matter that hints at potential tensions [8–10].

In this Letter, we determine the neutron skin of ^{208}Pb from a new type of probe. We use data collected in ^{208}Pb + ^{208}Pb collisions performed at ultrarelativistic energy at the CERN Large Hadron Collider (LHC). These collisions produce short-lived quark-gluon plasma [11–13] (QGP), the hot phase of quantum chromodynamics (QCD), which behaves like a near-ideal relativistic fluid [14,15] before fragmenting into observable particles. In high-energy scattering, interactions are mediated by gluons, such that the combined distribution of protons and neutrons (altogether called nucleons) within the colliding ^{208}Pb ions determines the shape and the size of the created QGP. Employing the latest advances in simulation and Bayesian inference tools within the hydrodynamic framework of heavy-ion collisions we reconstruct the geometry of the QGP by using the detected particle distributions. In conjunction with the precise knowledge of the proton density this enables us to place a tight constraint on the neutron skin of ^{208}Pb.

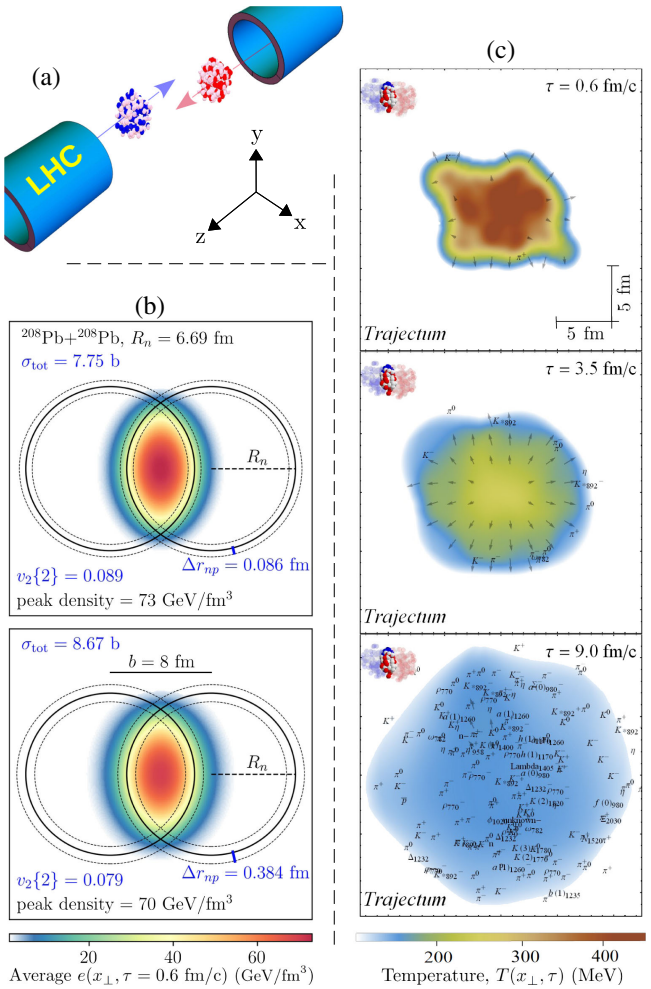

FIG. 1. Neutron skin and collective flow in relativistic nuclear collisions. (a) Two ions collide with impact parameter $b = 8$ fm. Both ions are Lorentz contracted by a factor $\gamma \approx 2500$, and the relevant dynamics hence effectively takes place in the transverse plane, $x_\perp = (x, y)$. (b) The collision deposits energy in the interaction region depending on the extent of the neutron skin of the ^{208}Pb nuclei. We consider $\Delta r_{np} = 0.086$ (top) and $\Delta r_{np} = 0.384$ fm (bottom). The neutron skin is varied by keeping the half-width neutron radius R_n constant while changing the neutron diffuseness, as displayed by the dotted lines [see also Eq. (2) below]. A larger neutron skin leads to a considerably larger total hadronic cross section, $\sigma_{\rm tot}$, and the resulting QGP is in addition more diffuse and less elliptical. (c) We show a single QGP evolving hydrodynamically and being converted into particles (marked in the figure with their respective symbols) as it cools, while expanding both in z and in the transverse plane. The observation of millions of such events leads to characteristic azimuthal anisotropies in the momentum distribution of the produced particles, the most important of which is quantified by the rms value of its second Fourier component, the elliptic flow $v_2\{2\}$, which reflects the ellipticity of the QGP.

The neutron skin and the quark-gluon plasma.—Our understanding of the QGP formed in ^{208}Pb + ^{208}Pb collisions is highly developed thanks to the wealth of experimental data collected in the past decade by all LHC experiments, and, in particular, by the ALICE experiment dedicated to nuclear physics [16]. Following Fig. 1, in an ultrarelativistic heavy-ion collision in the lab frame [Fig. 1(a)], interactions of gluons deposit energy density in the area of overlap in the so-called *transverse plane*, perpendicular to the beam direction [Fig. 1(b)]. The deposition of energy density depends on the collision's impact parameter b, on the structure of the colliding nuclei and on the dynamics of the interaction itself.

Phenomenological studies have established a picture where the colliding ions are treated, in each collision (or *event*), as a superposition of nucleons that participate in the interaction. Both boosted nuclei are thus associated with a profile of matter in the transverse plane, $\mathcal{T}_{\mathcal{L},\mathcal{R}}(x_\perp)$, given as the sum of their participant nucleon profiles, typically taken as Gaussians with a width denoted by w. The interaction process and the subsequent energy depositions are then parametrized following some flexible prescription which can be fine-tuned directly from experimental data. Here we use a T$_{\rm R}$ENTo-type ansatz for the energy density of the QGP [17,18],

$$e(x_\perp) \propto \left(\frac{\mathcal{T}_L(x_\perp - b/2)^p + \mathcal{T}_R(x_\perp + b/2)^p}{2}\right)^{q/p}, \qquad (1)$$

where L, R denote the two colliding ions, while p and q are model parameters. As the positions of the participant nucleons shaping the functions $\mathcal{T}_{L,R}$ are sampled in each collision from the neutron and proton densities in the ground state of the scattering ions, the energy density $e(x_\perp)$ is sensitive to their spatial distribution. This can be seen by eye in the density plot of Fig. 1(b), representing an average energy density over many collisions. The scenario where the colliding ^{208}Pb nuclei have a narrower neutron skin leads to a QGP with a sharper profile over the plane and a higher density peak.

Starting from the initial condition discussed in Fig. 1(b), the QGP then evolves as a relativistic viscous fluid (with transport properties, such as shear and bulk viscosities, that are also model parameters). For a single event, snapshots of the hydrodynamic expansion obtained using our hydrodynamic code are depicted in Fig. 1(c). Cooling of the QGP lasts until the confinement crossover is reached, after which at a fixed switching temperature the fluid is converted into a gas of QCD resonance states that can further rescatter or decay to stable particles. Out of this process, experiments can only detect final event-by-event stable particle spectra, typically denoted by

$$\frac{d^3N_{\rm ch}}{d^2\boldsymbol{p}_T d\eta} = \frac{d^2N_{\rm ch}}{dp_T d\eta}\frac{1}{2\pi}\left(1 + 2\sum_{n=1}^{\infty} v_n \cos n(\phi - \phi_n)\right),$$

where $\boldsymbol{p}_T$ is the transverse momentum, η is the particle pseudorapidity [$\eta \equiv -\ln\tan(\theta/2)$ with θ the polar angle in the $(x_\perp, z)$ plane of Fig. 1(a)], and the subscript ch indicates

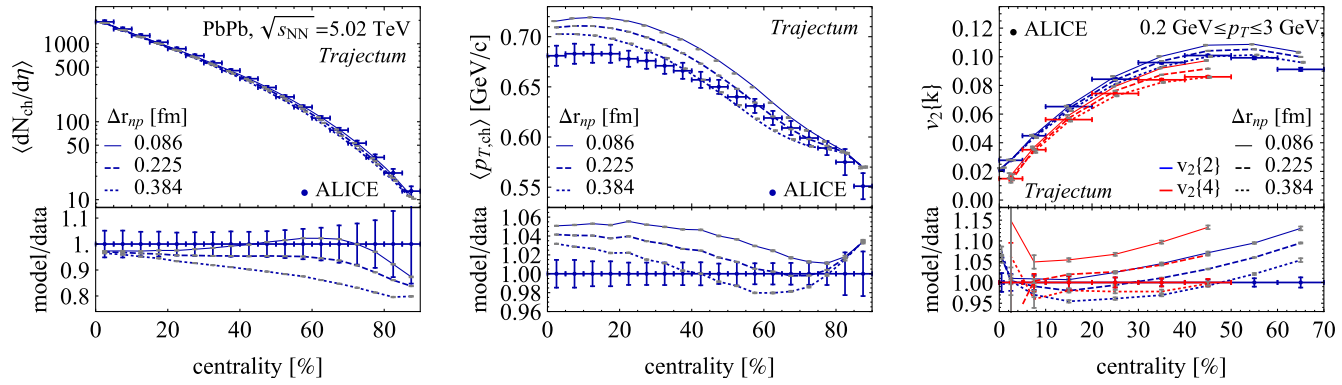

FIG. 2. Signature of the neutron skin on bulk particle production in ultrarelativisitic ^{208}Pb + ^{208}Pb collisions. Varying only the neutron skin size at our optimal parameter settings we show the charged particle multiplicity (left), the mean transverse momentum (middle), and the elliptic flow as measured by $v_2\{k\}$ (right) with a comparison to ALICE data [19,20]. A larger neutron skin leads to more collisions, but per collision the multiplicity is lower at larger centralities. The larger size of the QGP leads to a reduced transverse momentum on average. Smearing of the elliptical shape leads to reduced elliptic flow as measured by $v_2\{2\}$ and $v_2\{4\}$. Theoretical error bars are statistical only, experimental uncertainties include systematics as well.

that only charged particles are included. We have conveniently decoupled the spectrum into a distribution of transverse momenta, $p_T \equiv |\boldsymbol{p}_T|$, which quantifies the explosiveness of the QGP expansion, and an azimuthal component developed in Fourier modes, where v_n are the so-called anisotropic flow coefficients that quantify the anisotropy of the particle emission.

Experimentally the first step is to sort the collisions in centrality classes based on the number of particles that they produce, where 0% centrality corresponds to events with the highest number of particles at almost zero impact parameter. As a function of centrality one can then measure among others the distributions of p_T and v_n coefficients for different particle species (pions, kaons, protons, and more). This generates a wealth of experimental information from which the hydrodynamic model parameters (here, we have 26 in total) can be inferred. The central idea of this Letter is that of promoting the neutron skin of ^{208}Pb to a model parameter that we constrain from LHC data.

The neutron skin is introduced by considering variations in the neutron diffuseness, a_n, in the two-parameter Fermi distributions that model the point-neutron and point-proton densities in the colliding ^{208}Pb nuclei:

$$\rho_{n,p}(r) \propto \left[1 + \exp\left(\frac{r - R_{n,p}}{a_{n,p}}\right)\right]^{-1}. \tag{2}$$

We take $a_p = 0.448$, $R_p = 6.680$ (corresponding to an rms proton radius $r_p = 5.436$ fm), and $R_n = 6.690$ fm, which is motivated by the experimental result that the neutron skin is caused by a more diffuse profile rather than a larger half-width radius [1,2].

Before proceeding with a full Bayesian analysis we simulate the QGP formation and evolution for three different values of Δr_{np} while keeping all other model parameters fixed. First, a larger neutron skin leads to a larger total hadronic cross section, $\sigma_{\rm tot}$ [see Fig. 1(b) for an increase from 7.75 to 8.67 b], because it increases the overall number of events occurring at higher impact parameters.

We follow now Fig. 2, showing experimental and model results for quantities that characterize the bulk of particle production from the measured spectra. The larger $\sigma_{\rm tot}$ for the larger neutron skin induces larger impact parameters at the same centrality. As a consequence, fewer particles are produced for larger values of Δr_{np}, as clearly visible in the total multiplicity in Fig. 2 (left panel). A second effect of a larger skin, highlighted in Fig. 1(b), is that it leads to more diffuse QGP droplets, which leads to weaker pressure gradients and a slower hydrodynamic expansion. This translates into a lower average momentum of the detected particles, as seen in the middle panel of Fig. 2. In addition, Fig. 1 shows that a larger neutron skin reduces the ellipticity of the QGP. This leads to a reduction of the elliptic flow, measured in experiment as a two-particle azimuthal correlation ($v_2\{2\}$, the rms value of the distribution of v_2) or as a four-particle correlation ($v_2\{4\}$) İndeed, Fig. 2 (right) shows the expected reduction and moreover we find that a larger neutron skin enhances the difference between $v_2\{2\}$ and $v_2\{4\}$, which corresponds to larger elliptic flow fluctuations.

Bayesian inference of the ^{208}Pb *neutron skin.*—Because of the interplay and cross-correlations among parameters and observables, constraining the model from experiment requires advanced Bayesian analysis tools as pioneered in earlier works [15,21]. Our analysis makes use of 653 data points in ^{208}Pb + ^{208}Pb collisions and a single data point (the total cross section) of proton-nucleus (p + ^{208}Pb) collisions. We use 3000 design points for the Gaussian processes to emulate our collisions as a function of the 26-dimensional parameter space. See the Supplemental

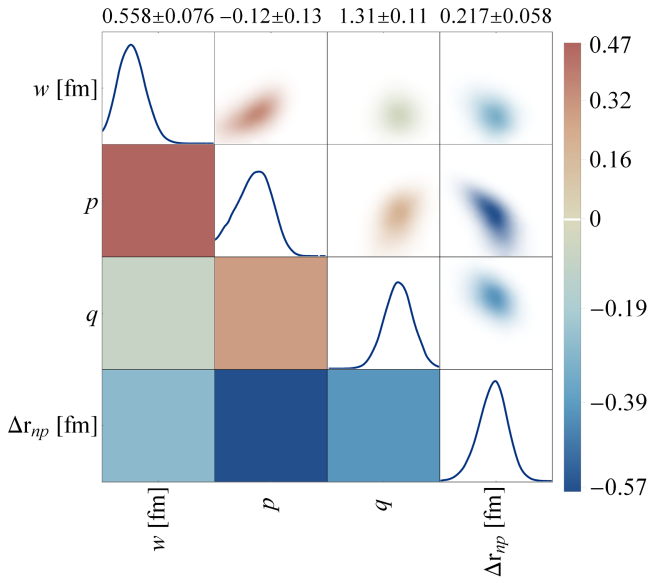

FIG. 3. Inferred neutron skin and energy-deposition parameters. We show the posterior distribution of the neutron skin Δr_{np}, the nucleon width w and the energy deposition parameters p and q, together with their expectation values (see top) and correlations. Uncertainties correspond to the standard deviations of the posterior distributions. Especially the p parameter [see Eq. (1)] is highly anticorrelated with Δr_{np}, as both have a strong effect on the centrality dependence of observables (see also Fig. 2).

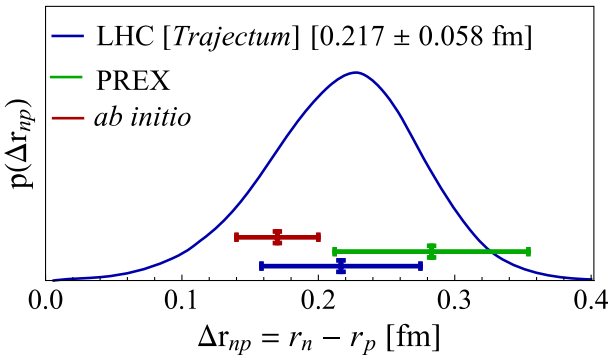

FIG. 4. State-of-the-art determinations of the neutron skin of ^{208}Pb. We show the final likelihood distribution of the neutron skin as determined from the LHC data as compared to the values obtained experimentally by the PREX Collaboration (including both experimental and theoretical uncertainties in the extraction) [6] and the estimate of *ab initio* nuclear theory (with an error bar corresponding to a 68% credibility interval) [7].

Material [22] for a specification of all data, parameters and their inferred distributions.

The posterior distributions are displayed in Fig. 3 for a subset of parameters that correlate highly with Δr_{np}. These are the parameters appearing in the energy deposition formula, Eq. (1), namely, the energy deposition parameters p and q, as well as the nucleon size, w. In fact, the p parameter and Δr_{np} are the most negatively correlated across our entire parameter space. This is not surprising, as both parameters strongly influence the centrality dependence of observables, whereby a larger neutron skin in particular affects off-central collisions by increasing the total cross section.

Here we briefly revisit Fig. 2, where the middle curve represents our most likely value estimate. In the Supplemental Material [22] we present the full posterior distributions of our set of 653 data points. There, it can also be seen that the reason for the mismatch between the computed $\langle p_T \rangle$ and experimental data in Fig. 2 lies in a slight overestimate of yield of protons, which comes with a larger p_T. There is also a significant posterior uncertainty in the anisotropic flow, which is dominated by the emulator uncertainty.

In Fig. 4 we put our new result in context of other state-of-the-art determinations of the skin of ^{208}Pb. From the posterior distribution we obtain $\Delta r_{np} = 0.217 \pm 0.058$ fm, corresponding to a pointlike rms neutron radius $r_n = 5.653 \pm 0.058$ fm. Our result is compatible with both the *ab initio* determination [7] and the PREX result [6], which is competitive in precision. With regards to the EOS of neutron matter, from the relation between Δr_{np} and the slope parameter, L, of the symmetry energy around the nuclear saturation density [41], we obtain $L = 79 \pm 39$ MeV, representing the first collider-based constraint on this parameter from high-energy data.

We comment now on the robustness of this result. The total $^{208}\mathrm{Pb} + {}^{208}\mathrm{Pb}$ and $p + {}^{208}\mathrm{Pb}$ cross sections [42,43] pose important constraints on the neutron skin. Indeed, excluding these two measurements we obtain $\Delta r_{np} = 0.31 \pm 0.10$ fm, whereas using exclusively these two data points results in $\Delta r_{np} = 0.03 \pm 0.12$ fm. Our result comes hence from constraints due to a combination of observables, where the cross section prefers a smaller neutron skin, while other observables prefer a larger value (this is similar for w [44]). For the first time in Bayesian analyses we include the ρ_2 observable [45,46], a sensitive probe of the initial conditions [44,47–50], which measures the correlation between $v_2\{2\}$ and $\langle p_T \rangle$. Without this observable, the analysis yields a consistent result, $\Delta r_{np} = 0.243 \pm 0.059$ fm. Also, as introduced in Ref. [44], we weight the targeted observables according to a prescription that models unknown theoretical uncertainty with respect to p_T-differential observables in particular. Turning this weighting off, we find a consistent albeit slightly smaller neutron skin, $\Delta r_{np} = 0.160 \pm 0.057$ fm.

Further indication of the robustness of our finding comes from the fact that targeting a subset of p_T-integrated-only observables, corresponding to 233 ALICE data points, we obtain $\Delta r_{np} = 0.216 \pm 0.057$ fm. This suggests that the extraction of Δr_{np} is likely insensitive to theoretical uncertainties in the particlization of the QGP at the switching temperature [51]. Lastly, we note that our T$_\mathrm{R}$ENTo ansatz of Eq. (1) is very versatile, and may lead

to a relatively conservative estimate of the uncertainty on Δr_{np}. Implementing in the future a model of initial conditions motivated by first-principles arguments and with fewer parameters [52], may lead to stronger constraints than presented here.

Future skin determinations at the LHC.—Albeit computationally expensive, it would be interesting to vary the full neutron profile, by changing R_n, or via a multiparameter function as in Ref. [2]. The Supplemental Material [22] presents an exploratory study of this kind. Increasing the neutron half-width radius does not affect the average multiplicity and the elliptic flow, but leads to a decrease in the mean transverse momentum and a higher hadronic cross section. We speculate, thus, that a more complete analysis could eventually lead to a slightly smaller neutron skin.

We expect our analysis to trigger a program of complementary measurements of skin effects at the LHC. A method pioneered by the STAR Collaboration utilizes the photoproduction of vector mesons in ultraperipheral nucleus-nucleus collisions to infer the average gluon density in the colliding nuclei, and hence the neutron skins [53]. The extracted skin of ^{197}Au is in good agreement with nuclear theory predictions [54]. Therefore, the same method could be exploited at the LHC to perform an independent extraction of the skin of ^{208}Pb.

In addition, the global analysis presented here uses so-called *soft* observables that depend on particles with transverse momentum of order of the QCD deconfinement temperature, around 150 MeV. With high-luminosity LHC runs it may be possible to constrain the neutron skin as well via *hard* observables, such as high transverse momentum electroweak bosons [55,56]. The charge of the produced electroweak bosons can serve as a direct probe of the number of neutron-neutron interactions. By selecting collisions at relatively large impact parameter, it is then possible to determine the dominance of neutrons at the outer edges of the ^{208}Pb nucleus.

It is likely that the nucleus ^{48}Ca and other ions will be collided at the high-luminosity LHC in the next decade [57]. This will enable an extended analysis that, in particular, can be compared with the dedicated CREX measurement of the neutron skin of ^{48}Ca [58]. Comparing many different collision systems will furthermore permit us to study ratios of observables that cancel most of the systematic theoretical uncertainties [59–62], leading to improved determinations of Δr_{np} across the nuclear chart.

We acknowledge discussions with the participants of INT-23-1a, "Intersection of nuclear structure and high-energy nuclear collisions," and the hospitality of the Institute for Nuclear Theory, Seattle. We thank, in particular, Rituparna Kanungo for interesting discussions. We thank Krishna Rajagopal for comments on the manuscript. G. G. is supported by the Deutsche Forschungsgemeinschaft (DFG, German Research Foundation) under Germany's Excellence Strategy EXC 2181/1–390900948 (the Heidelberg STRUCTURES Excellence Cluster), SFB 1225 (ISOQUANT) and FL 736/3-1. G. N. is supported by the U.S. Department of Energy, Office of Science, Office of Nuclear Physics under grant Contract No. DE-SC0011090.

[1] A. Trzcinska, J. Jastrzebski, P. Lubinski, F. J. Hartmann, R. Schmidt, T. von Egidy, and B. Klos, Phys. Rev. Lett. **87**, 082501 (2001).
[2] J. Zenihiro *et al.*, Phys. Rev. C **82**, 044611 (2010).
[3] B. A. Brown, Phys. Rev. Lett. **85**, 5296 (2000).
[4] C. J. Horowitz and J. Piekarewicz, Phys. Rev. Lett. **86**, 5647 (2001).
[5] H. De Vries, C. W. De Jager, and C. De Vries, At. Data Nucl. Data Tables **36**, 495 (1987).
[6] D. Adhikari *et al.* (PREX Collaboration), Phys. Rev. Lett. **126**, 172502 (2021).
[7] B. Hu *et al.*, Nat. Phys. **18**, 1196 (2022).
[8] F. J. Fattoyev, J. Piekarewicz, and C. J. Horowitz, Phys. Rev. Lett. **120**, 172702 (2018).
[9] B. T. Reed, F. J. Fattoyev, C. J. Horowitz, and J. Piekarewicz, Phys. Rev. Lett. **126**, 172503 (2021).
[10] R. Essick, I. Tews, P. Landry, and A. Schwenk, Phys. Rev. Lett. **127**, 192701 (2021).
[11] P. Braun-Munzinger and J. Stachel, Nature (London) **448**, 302 (2007).
[12] D. A. Teaney, Viscous hydrodynamics and the quark gluon plasma, in *Quark-Gluon Plasma 4*, edited by R. C. Hwa and X.-N. Wang (World Scientific, Singapore, 2010), pp. 207–266.
[13] F. G. Gardim, G. Giacalone, M. Luzum, and J.-Y. Ollitrault, Nat. Phys. **16**, 615 (2020).
[14] P. Romatschke and U. Romatschke, *Relativistic Fluid Dynamics In and Out of Equilibrium*, Cambridge Monographs on Mathematical Physics (Cambridge University Press, Cambridge, England, 2019).
[15] J. E. Bernhard, J. S. Moreland, and S. A. Bass, Nat. Phys. **15**, 1113 (2019).
[16] ALICE Collaboration, arXiv:2211.04384.
[17] J. S. Moreland, J. E. Bernhard, and S. A. Bass, Phys. Rev. C **92**, 011901(R) (2015).
[18] G. Nijs and W. van der Schee, arXiv:2304.06191.
[19] S. Acharya *et al.* (ALICE Collaboration), Phys. Lett. B **793**, 420 (2019).
[20] S. Acharya *et al.* (ALICE Collaboration), J. High Energy Phys. 07 (2018) 103.
[21] E. Sangaline and S. Pratt, Phys. Rev. C **93**, 024908 (2016).
[22] See Supplemental Material at http://link.aps.org/supplemental/10.1103/PhysRevLett.131.202302, which contains Refs. [23–40], for a specification of all data, parameters with ranges, their inferred distributions as well as a variation of R_n.
[23] J. Weil *et al.* (SMASH Collaboration), Phys. Rev. C **94**, 054905 (2016).
[24] D. Oliinychenko, V. Steinberg, J. Weil, M. Kretz, J. Staudenmaier, S. Ryu, A. Schäfer, J. Rothermel, J. Mohs, F. Li, H. E. (Petersen), L. Pang, D. Mitrovic,

A. Goldschmidt, L. Geiger, J.-B. Rose, J. Hammelmann, and L. Prinz, smash-transport/smash: Smash-1.8 (2020).
[25] T. Sjostrand, S. Mrenna, and P. Z. Skands, Comput. Phys. Commun. **178**, 852 (2008).
[26] B. Bally, M. Bender, G. Giacalone, and V. Somà, Phys. Rev. Lett. **128**, 082301 (2022).
[27] F. Cooper and G. Frye, Phys. Rev. D **10**, 186 (1974).
[28] S. Pratt and G. Torrieri, Phys. Rev. C **82**, 044901 (2010).
[29] K. Aamodt *et al.* (ALICE Collaboration), Phys. Rev. Lett. **106**, 032301 (2011).
[30] J. Adam *et al.* (ALICE Collaboration), Phys. Rev. Lett. **116**, 222302 (2016).
[31] B. Abelev *et al.* (ALICE Collaboration), Phys. Rev. C **88**, 044910 (2013).
[32] J. Adam *et al.* (ALICE Collaboration), Phys. Rev. C **94**, 034903 (2016).
[33] B. B. Abelev *et al.* (ALICE Collaboration), Eur. Phys. J. C **74**, 3077 (2014).
[34] J. Adam *et al.* (ALICE Collaboration), Phys. Rev. Lett. **116**, 132302 (2016).
[35] J. Adam *et al.* (ALICE Collaboration), J. High Energy Phys. 09 (2016) 164.
[36] M. Aaboud *et al.* (ATLAS Collaboration), J. High Energy Phys. 01 (2020) 051.
[37] D. J. Earl and M. W. Deem, Phys. Chem. Chem. Phys. **7**, 3910 (2005).
[38] D. Foreman-Mackey, D. W. Hogg, D. Lang, and J. Goodman, Publ. Astron. Soc. Pac. **125**, 306 (2013).
[39] ALICE Collaboration, arXiv:2204.10148.
[40] O. Garcia-Montero, J. Staudenmaier, A. Schäfer, J. M. Torres-Rincon, and H. Elfner, Phys. Rev. C **105**, 064906 (2022).
[41] X. Viñas, M. Centelles, X. Roca-Maza, and M. Warda, Eur. Phys. J. A **50**, 27 (2014).
[42] ALICE Collaboration, arXiv:2204.10148.
[43] V. Khachatryan *et al.* (CMS Collaboration), Phys. Lett. B **759**, 641 (2016).
[44] G. Nijs and W. van der Schee, Phys. Rev. Lett. **129**, 232301 (2022).
[45] P. Bozek, Phys. Rev. C **93**, 044908 (2016).
[46] ATLAS, Phys. Rev. C **107**, 054910 (2023).
[47] P. Bozek and H. Mehrabpour, Phys. Rev. C **101**, 064902 (2020).
[48] B. Schenke, C. Shen, and D. Teaney, Phys. Rev. C **102**, 034905 (2020).
[49] G. Giacalone, F. G. Gardim, J. Noronha-Hostler, and J.-Y. Ollitrault, Phys. Rev. C **103**, 024909 (2021).
[50] G. Giacalone, B. Schenke, and C. Shen, Phys. Rev. Lett. **128**, 042301 (2022).
[51] D. Everett, W. Ke, J. F. Paquet, G. Vujanovic, S. A. Bass *et al.* (JETSCAPE Collaboration), Phys. Rev. C **103**, 054904 (2021).
[52] M. R. Heffernan, C. Gale, S. Jeon, and J.-F. Paquet, arXiv: 2302.09478.
[53] M. Abdallah *et al.* (STAR Collaboration), Sci. Adv. **9**, eabq3903 (2023).
[54] B. Bally, G. Giacalone, and M. Bender, Eur. Phys. J. A **59**, 58 (2023).
[55] H. Paukkunen, Phys. Lett. B **745**, 73 (2015).
[56] G. Aad *et al.* (ATLAS Collaboration), Eur. Phys. J. C **79**, 935 (2019).
[57] Z. Citron *et al.*, CERN Yellow Rep. Monogr. **7**, 1159 (2019).
[58] D. Adhikari *et al.* (CREX Collaboration), Phys. Rev. Lett. **129**, 042501 (2022).
[59] H.-j. Xu, H. Li, X. Wang, C. Shen, and F. Wang, Phys. Lett. B **819**, 136453 (2021).
[60] J. Jia and C. Zhang, Phys. Rev. C **107**, L021901 (2023).
[61] G. Nijs and W. van der Schee, SciPost Phys. **15**, 041 (2023).
[62] J. Jia, G. Giacalone, and C. Zhang, Phys. Rev. Lett. **131**, 022301 (2023).